

# Thermochromic Printable and Multicolor Polymeric Composite Based on Hybrid Organic–Inorganic Perovskite

Marco Cinquino, Carmela Tania Prontera, Antonella Giuri, Marco Pugliese,\* Roberto Giannuzzi, Antonio Maggiore, Davide Altamura, Fabrizio Mariano, Giuseppe Gigli, Carola Esposito Corcione, Cinzia Giannini, Aurora Rizzo, Luisa De Marco,\* and Vincenzo Maiorano

Hybrid organic–inorganic perovskites (PVKs) are among the most promising materials for optoelectronic applications thanks to their outstanding photophysical properties and easy synthesis. Herein, a new PVK-based thermochromic composite is demonstrated. It can reversibly switch from a transparent state (transmittance > 80%) at room temperature to a colored state (transmittance < 10%) at high temperature, with very fast kinetics, taking only a few seconds to go from the bleached to the colored state (and vice versa). X-ray diffraction, Fourier-transform infrared spectroscopy, differential scanning calorimetry, rheological, and optical measurements carried out during heating/cooling cycles reveal that thermochromism in the material is based on a reversible process of PVK disassembly/assembly mediated by intercalating polymeric chains, through the formation and breaking of hydrogen bonds between polymer and perovskite. Therefore, differently from other thermochromic perovskites, that generally work with the adsorption/desorption of volatile molecules, the system is able to perform several heating/cooling cycles regardless of environmental conditions. The color and transition temperature (from 70 to 120 °C) can be tuned depending on the type of perovskite. Moreover, this thermochromic material is printable and can be deposited by cheap techniques, paving the way for a new class of smart coatings with an unprecedented range of colors.

received increasing interest in recent years because of its wide application in smart coating materials,<sup>[1,2]</sup> textiles,<sup>[3–5]</sup> conductive elastomers,<sup>[6]</sup> energy-saving materials,<sup>[7,8]</sup> and temperature-indicating materials.<sup>[9,10]</sup> Indeed, the deposition of thermochromic compounds on a substrate provides it with new functionalities, such as the possibility of generating a visual safety warning in case of abnormal heating of equipment during operation. For example, they can be implemented in systems where conventional temperature measurement tools cannot be used, such as parts of high-tension apparatus, continuously running equipment, or dangerous environments.


Commonly employed thermochromic materials are liquid crystals (LCs),<sup>[11,12]</sup> leuco dyes,<sup>[13,14]</sup> and some inorganic compounds based on vanadium dioxide.<sup>[15–17]</sup> The latter shows a good thermochromic effect in the near-infra-red (IR) region ( $\lambda > 900$  nm) and low modulation ability in the visible range at transition temperature  $\geq 65$  °C.<sup>[16,18–22]</sup> Unfortunately, its deposition requires expensive vacuum-based techniques,<sup>[23–26]</sup> which limit its

wide use for practical applications. LCs show thermochromic behavior at lower transition temperatures with good modulation of transmittance in the visible range. The disadvantages of LCs are their slow transition dynamics and the need for rigorous encapsulation because leakage problems can occur

## 1. Introduction

Thermochromism is the property of some materials to reversibly change their color upon temperature variations. It can be exploited for sensing and monitoring applications and has

M. Cinquino, C. T. Prontera, A. Giuri, M. Pugliese, R. Giannuzzi, A. Maggiore, F. Mariano, G. Gigli, A. Rizzo, L. De Marco, V. Maiorano  
CNR NANOTEC — Institute of Nanotechnology  
Nationa Research Council  
c/o Campus Ecotekne, Via Monteroni, Lecce 73100, Italy  
E-mail: marco.pugliese@nanotec.cnr.it; luisa.demarco@nanotec.cnr.it

 The ORCID identification number(s) for the author(s) of this article can be found under <https://doi.org/10.1002/adma.202307564>

© 2023 The Authors. Advanced Materials published by Wiley-VCH GmbH. This is an open access article under the terms of the Creative Commons Attribution License, which permits use, distribution and reproduction in any medium, provided the original work is properly cited.

DOI: 10.1002/adma.202307564

M. Cinquino, R. Giannuzzi, G. Gigli  
Dipartimento di Matematica e Fisica E. De Giorgi, Università Del Salento  
Campus Ecotekne  
via Monteroni, Lecce 73100, Italy  
D. Altamura, C. Giannini  
Institute of Crystallography  
CNR-IC  
Via Amendola 122/O, Bari 70126, Italy  
C. Esposito Corcione  
Dipartimento di Ingegneria dell'Innovazione  
Università Del Salento  
Campus Ecotekne  
via Monteroni, Lecce 73100, Italy

during their utilization, resulting in a dramatic decrease in their performance.<sup>[11,12]</sup> Finally, leuco dyes have a transition temperature lower than 50 °C, although show limited color change.<sup>[27,28]</sup> As the LCs, they must be encapsulated to avoid solvents leakage and unwanted environmental reactions.<sup>[29,30]</sup>

Recently, organic–inorganic perovskites (PVKs), which are emerging hybrid semiconductors suitable for photovoltaic,<sup>[31–33]</sup> photodetection,<sup>[34,35]</sup> light emission,<sup>[36]</sup> and photonic<sup>[37–41]</sup> applications, have shown interesting thermochromic properties.<sup>[42–47]</sup>

The origin of thermochromism in hybrid perovskites was attributed to changes in their crystalline structure induced by a slight modulation/distorsion of the lattice<sup>[48–50]</sup> or by adsorption/desorption of volatile molecules such as water, methylamine, or solvents that alter the perovskite's crystal lattice.<sup>[44–47]</sup> Regarding the first mechanism, thermochromism was observed in copper-based layered perovskites that show a reversible color change from orange at room temperature to red at high temperature<sup>[48]</sup> or in full inorganic perovskites, such as Cs<sub>3</sub>Sb<sub>2</sub>I<sub>9</sub><sup>[49]</sup> and Cs<sub>2</sub>AgBiBr<sub>6</sub><sup>[50]</sup> that change color from red to brown. This behavior is attributed to phase transitions with slight changes in the interatomic distances and/or lattice expansion. Although these systems have the advantage of working in solid-state, the difference in coloration between the two phases is relatively small, which may restrict the application of these materials. On the other hand, the second mechanism yielded better color variation by exploiting thermochromism dependent on vapor adsorption. At room temperature perovskite and volatile molecules (such as methylamine<sup>[46]</sup> or more often water<sup>[42,44,45,47,51]</sup>) react to form a transparent nonperovskite compound, while at high-temperature volatile molecules desorb from the crystalline structure leaving a dark reddish-brown thin film of perovskite. Wheeler et al. demonstrated that photothermal heating at 60 °C causes the MAPbI<sub>3</sub>-methylamine complex to change from a transparent state (68% visible transmittance) to a photovoltaic colored state (less than 3% visible transmittance). This device can only operate in a controlled atmosphere, so it must be sealed and equipped with a methylamine reservoir chamber, greatly complicating its application as a thermochromic smart window.<sup>[46]</sup> Lin et al. showed a Cesium Lead iodide/bromide perovskite (CsPbI<sub>3–x</sub>Br<sub>x</sub>) thin film that undergoes thermally driven and moisture-mediated transitions between a transparent phase (82% visible transmittance) and a colored perovskite phase (35% visible transmittance). The transition occurs at a temperature > 100 °C, is quite slow (taking several minutes or hours) and is strongly dependent on the ambient moisture.<sup>[42]</sup> Very recently, Rosales et al.<sup>[52]</sup> developed a thermochromic perovskite window based on MAPbI<sub>3–x</sub>Cl<sub>x</sub> that can achieve a transmittance change of 53% at the ideal temperature of 20–27 °C by employing methanol as the intercalating solvent and including polyacrylic acid as additive. Although the operating temperature is among the lowest reported to date, the operating mechanism relies on the intercalation of solvent vapor, which makes tricky the implementation of the device. Moreover, no data are available on the kinetics and hysteresis properties, which are crucial in some applications, such as smart windows. These aspects have been investigated by some researchers.<sup>[44,45]</sup> Among them, Liu et al., proposed a thermochromic hydrated perovskite (H-MAPbI<sub>3–x</sub>Cl<sub>x</sub>) that allows for a low transition temperature (30–50 °C), narrow

hysteresis (7–13 °C), and short transition time (1–4 min) by controlling environmental humidity.<sup>[45]</sup>

In this work, we present a thermochromic composite based on perovskite that overcomes the shortcomings of PVK systems, allowing large chromatic variation without being dependent on the presence of water or other vapors.

The composite consists of a low dimensional perovskite having formula (C<sub>4</sub>H<sub>9</sub>NH<sub>3</sub>)<sub>2</sub>(CH<sub>3</sub>NH<sub>3</sub>)<sub>n–1</sub>Pb<sub>n</sub>I<sub>3n+1</sub> (with *n* = 1, 2, and 3) and a copolymer (**Pluronic L-61**). It exhibits a transmittance modulation of about 80% in a few seconds at temperature 70–120 °C, with a hysteresis of 19 °C.

This process takes place with the same efficiency whether in air, vacuum, or nitrogen, regardless of the nature of the working atmosphere. As a further benefit, our system allows modulating the color of the thermochromic device by using PVK with different *n* values. In addition, this material is in the form of printable ink and can be easily deposited through cheap, vacuum-free, and large-area techniques such as inkjet printing, roll-to-roll, and screen printing, becoming a coating material that does not need encapsulation and is suitable for covering different types of surfaces such as glass, wood, plastic, metals, or textiles.

All these advantages, make the PVK-polymeric thermochromic ink proposed in this study a competitive alternative among all the thermochromic materials reported so far.

## 2. Results and Discussion

Two-dimensional perovskites (2D-PVKs) are today considered extremely promising because, compared to their 3D counterparts, are characterized by better stability in environmental conditions<sup>[53,54]</sup> and larger degrees of structural freedom.<sup>[55]</sup> In particular, we use Ruddlesden–Popper halide perovskites (RPPs) having the general formula (R-NH<sub>3</sub>)<sub>2</sub>(A)<sub>n–1</sub>M<sub>n</sub>X<sub>3n+1</sub> and *n* = 1, 2, and 3; R-NH<sub>3</sub> is a butylammonium (BA<sup>+</sup>), A is methylammonium, (MA<sup>+</sup>), M is Pb<sup>2+</sup>, and X is the I<sup>–</sup> halide. As shown in **Figure 1a**, the chemical structure consists of inorganic layers of corner-sharing PbI<sub>6</sub><sup>4–</sup> octahedra sandwiched between long-chain organic cations which are linked to PbI<sub>6</sub><sup>4–</sup> by an ionic bond between the ammonium groups and the iodide anions. RPPs have a multiple quantum well structure<sup>[37,39,41,56]</sup> where inorganic and organic layers serve as energetic “well” and “barriers”, respectively, and the variable “*n*” indicates the number of PbI<sub>6</sub><sup>4–</sup> layers stacked between two R-NH<sub>3</sub><sup>+</sup>. Varying the number of inorganic layers “*n*” allows modulating the bandgap energy and, consequently, the material's optical properties, such as absorption, emission, and color.<sup>[33,57–59]</sup>

Our polymeric thermochromic composite consists of a (C<sub>4</sub>H<sub>9</sub>NH<sub>3</sub>)<sub>2</sub>(CH<sub>3</sub>NH<sub>3</sub>)<sub>n–1</sub>Pb<sub>n</sub>I<sub>3n+1</sub> (with *n* = 1, 2, and 3) perovskite and a nonionic block copolymer (**Pluronic L-61**) with structure PEG-PPG-PEG (HO(C<sub>2</sub>H<sub>4</sub>O)<sub>a</sub>-(C<sub>3</sub>H<sub>6</sub>O)<sub>b</sub>-(C<sub>2</sub>H<sub>4</sub>O)<sub>a</sub>H) where *a* = 2 and *b* = 31.

It is prepared by mixing perovskite precursors solution and Pluronic L-61 in tetrahydrofuran (THF) and it is deposited by inkjet printing on glass substrates, followed by thermal annealing in air at 120 °C for 10 min. All fabrication details are outlined in the Experimental Section. During the annealing step, the solvents completely evaporate and the composite takes on different colors depending on the value of inorganic layers (*n*).<sup>[56]</sup> At the end of this step, the composite is brought back to room

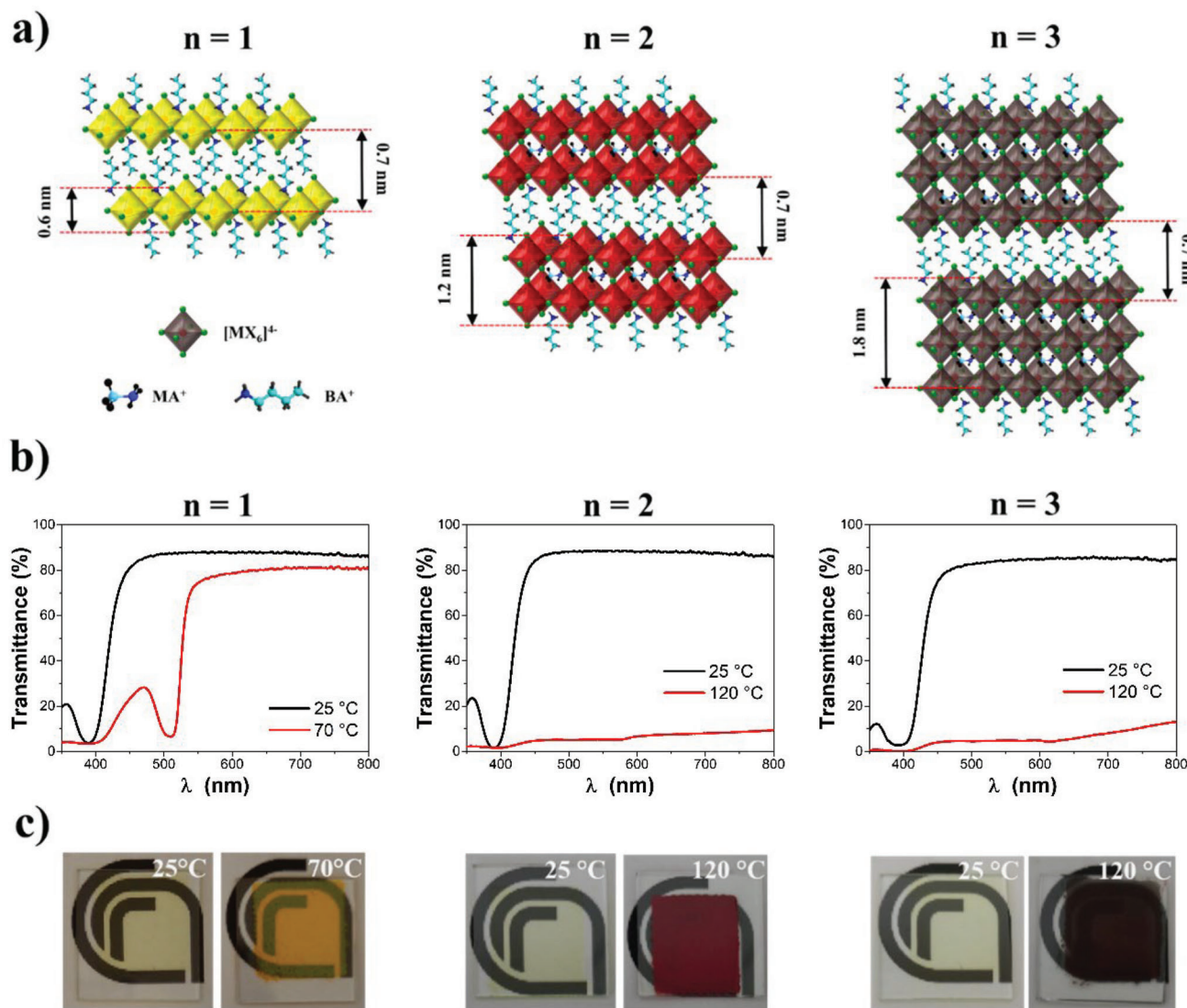


**Figure 1.** a) Schematic illustration of  $(\text{C}_4\text{H}_9\text{NH}_3)_2(\text{CH}_3\text{NH}_3)_{n-1}\text{Pb}_n\text{I}_{3n+1}$  (with  $n = 1, 2,$  and  $3$ ). b) Transmittance spectra and c) photographs of thermochromic  $(\text{C}_4\text{H}_9\text{NH}_3)_2(\text{CH}_3\text{NH}_3)_{n-1}\text{Pb}_n\text{I}_{3n+1}$  composite with  $n = 1, n = 2,$  and  $n = 3$  on glass substrate.

temperature where, regardless of the value of  $n$ , it becomes a pale-yellow transparent phase.

The three composites exhibit reversible thermochromic properties: the color of the films completely and quickly changes when heated at  $70\text{ }^\circ\text{C}$  in the case of  $(\text{C}_4\text{H}_9\text{NH}_3)_2\text{PbI}_4$  ( $n = 1$ ), becoming yellow, or at  $120\text{ }^\circ\text{C}$  in the case of  $(\text{C}_4\text{H}_9\text{NH}_3)_2(\text{CH}_3\text{NH}_3)_{n-1}\text{Pb}_n\text{I}_{3n+1}$  (with  $n = 2$  and  $3$ ), turning red and dark brown, respectively (see Figure 1c).

The optical transmittance of the three composites was measured at room temperature (transparent state) and high temperature (colored state) and the spectra are shown in Figure 1b, while their absorption spectra and luminous transmittance are reported in the Supporting Information (Figure S1 and Table S1). At room temperature, the pale-yellow films have high transmittance ( $>85\%$ ) in the range of  $450\text{--}800\text{ nm}$  (air was used as reference), while at high temperatures we observe a strong reduction of the transmittance. As shown in Figure 1b,

$(\text{C}_4\text{H}_9\text{NH}_3)_2\text{PbI}_4$  ( $n = 1$ ) and  $(\text{C}_4\text{H}_9\text{NH}_3)_2(\text{CH}_3\text{NH}_3)\text{Pb}_2\text{I}_7$  ( $n = 2$ ) achieve  $\Delta T_{\text{max}} = 80.8\%$  and  $83.2\%$ , respectively, at  $510\text{ nm}$ ;  $(\text{C}_4\text{H}_9\text{NH}_3)_2(\text{CH}_3\text{NH}_3)_2\text{Pb}_3\text{I}_{10}$  ( $n = 3$ ) reaches  $\Delta T_{\text{max}} = 80.7\%$  at  $619\text{ nm}$ . All the composites show very efficient tuning of the visible light transmittance and a strong chromatic variation, greater than other perovskites<sup>[42,45,46]</sup> and comparable to the most efficient thermochromic materials.

Moreover, our composite exhibits very fast kinetics, taking only a few seconds to switch from bleached to colored state (and vice versa). As an example, the transition times of  $(\text{C}_4\text{H}_9\text{NH}_3)_2(\text{CH}_3\text{NH}_3)\text{Pb}_2\text{I}_7$  ( $n = 2$ ) are shown in Figure 2, while the movies showing the color change of the three composites during heating are reported in the Supporting Information. As soon as the composite is heated the coloring process starts immediately and, in a few seconds (less than 15), all the material is in the colored state (see Figure 2a); the bleaching process takes a slightly longer time: it starts 60 s after the sample is removed

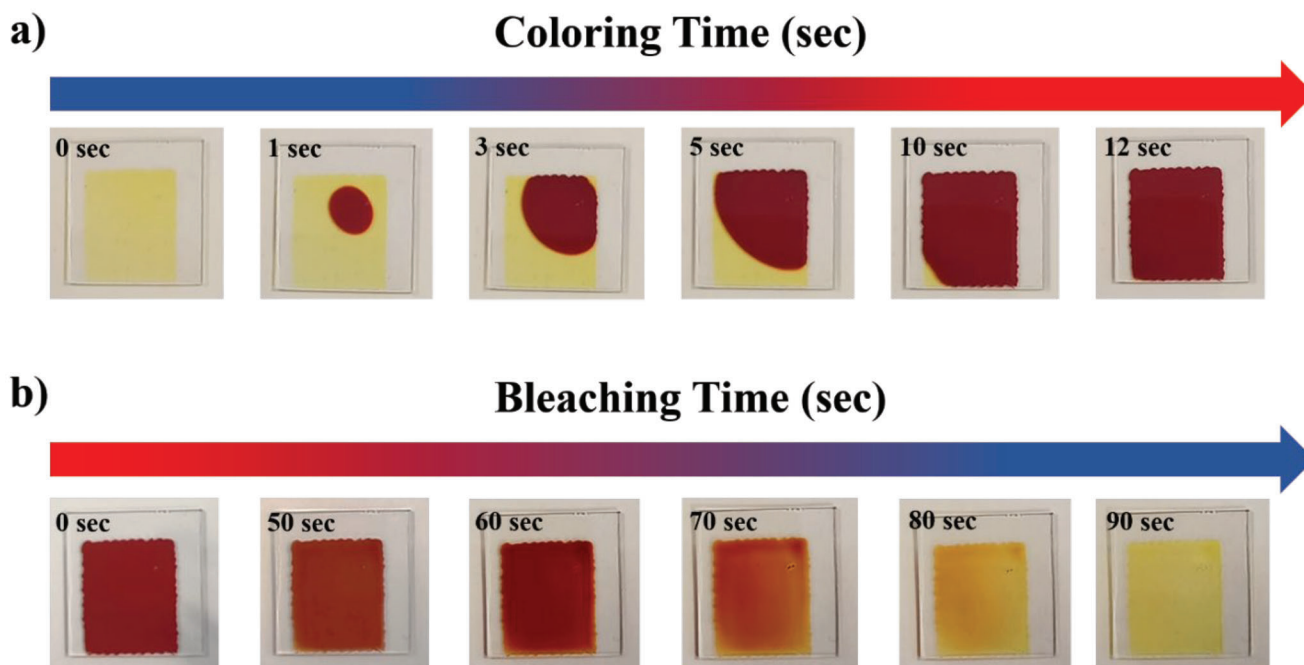


**Figure 2.** a) Coloring and b) bleaching kinetics of  $(\text{C}_4\text{H}_9\text{NH}_3)_2(\text{CH}_3\text{NH}_3)\text{Pb}_2\text{I}_7$  ( $n = 2$ ).

from the hot plate and is completed in 90 s (see Figure 2b). It seems that the slightly slow discoloration dynamics are affected by the thermal inertia of the glass substrate and composite (as they cool slowly, the bleaching step is delayed). Notwithstanding, the system presented here shows much faster dynamics than other thermochromic perovskites.<sup>[43,45]</sup>

We hypothesize that the observed thermochromism is related to a reversible disassembly and assembly of the perovskite driven by the intercalation or deintercalation of polymeric chains in the perovskite crystalline structure.

To better understand this aspect, we investigated the chemical bonds between polymer and perovskite through Fourier-transform infrared spectroscopy (FT-IR). The FT-IR spectra of the composite  $n = 2$  (consisting of  $(\text{C}_4\text{H}_9\text{NH}_3)_2(\text{CH}_3\text{NH}_3)\text{Pb}_2\text{I}_7$  and Pluronic L61) acquired at room temperature (RT) and 120 °C are reported in Figure 3a.

It is possible to identify the characteristic bands of the Pluronic backbone corresponding to the C–H asymmetric and symmetric stretching at 2972 and 2871  $\text{cm}^{-1}$ , respectively, and to the C–O stretching between 1000 and 1200  $\text{cm}^{-1}$ .<sup>[60,61]</sup> Moreover, we can recognize the vibrational modes corresponding to the methylammonium (MAI) and butylammonium (BAI) organic cations: C–H asymmetric and symmetric stretching at 2970–2870  $\text{cm}^{-1}$ , N–H stretching between 3000 and 3200  $\text{cm}^{-1}$ , N–H bending at 1550–1650  $\text{cm}^{-1}$ , and C–N stretching at 920–930  $\text{cm}^{-1}$ .<sup>[52]</sup>

If we compare the two spectra taken at RT and 120 °C, we can observe some differences. In particular, we focus on the N–H stretching modes at 3000–3200  $\text{cm}^{-1}$  and the N–H bending modes at 1550–1650  $\text{cm}^{-1}$  because they are rather isolated, not overlapped with the Pluronic peaks, and can give an idea of the environment in which the organic cations of the perovskite (MAI and BAI) are in the colored or bleached phase. After heating from RT to 120 °C, the N–H stretching mode shifts from

3172 to 3110  $\text{cm}^{-1}$ , while the N–H bending mode shifts from 1620 to 1574  $\text{cm}^{-1}$ . These redshifts toward lower wavenumbers indicate that the bending vibration is weaker at high temperature and the N–H bonds are stretched.<sup>[62]</sup> It is known that the vibrational modes of the N–H bonds are influenced by the H-bond they form with their surroundings and are subject to opposing forces of contraction and stretching.<sup>[63]</sup> Thus, FTIR analysis suggests that the binding environment of MAI and BAI changes with temperature: at high temperature, as the perovskite forms, the interaction between the N–H of MAI and BAI and the Pb–I structure leads to stretching of the N–H bonds,<sup>[62,64]</sup> while at RT the N–H bonds are shortened and strengthened.<sup>[52,65]</sup> This is justified by the nature of the H-bond formed between BAI/MAI and the Pluronic: the ether and/or hydroxyl groups of the polymer donate electronic density, causing a net gain in electronic density in the N–H bond region and resulting in strengthening of the N–H bond with blueshift of the vibrational modes.<sup>[52]</sup>

Therefore, we can reasonably state that at RT, stable hydrogen bonds are formed between Pluronic and the  $\text{NH}_3^+$  of MAI and BAI, stripping organic cations from the perovskite and giving rise to the thermodynamically most stable phase, the bleached one. When we heat the system, we provide the energy to break these hydrogen bonds, allowing the formation of perovskite. Thus, the equilibrium between the two phases moves toward the bleached or colored phase when the strength and number of interactions between the intercalating polymer chains and perovskite increase or decrease, respectively.

To further investigate this point, we performed differential scanning calorimetry (DSC) on our thermochromic composites. The sample  $n = 2$  has been subjected to a thermal cycle consisting of three steps: first heating, second cooling, and third heating (see the thermograms in Figure 3b,c and the data in Table S2, Supporting Information). It is possible to observe a well-defined

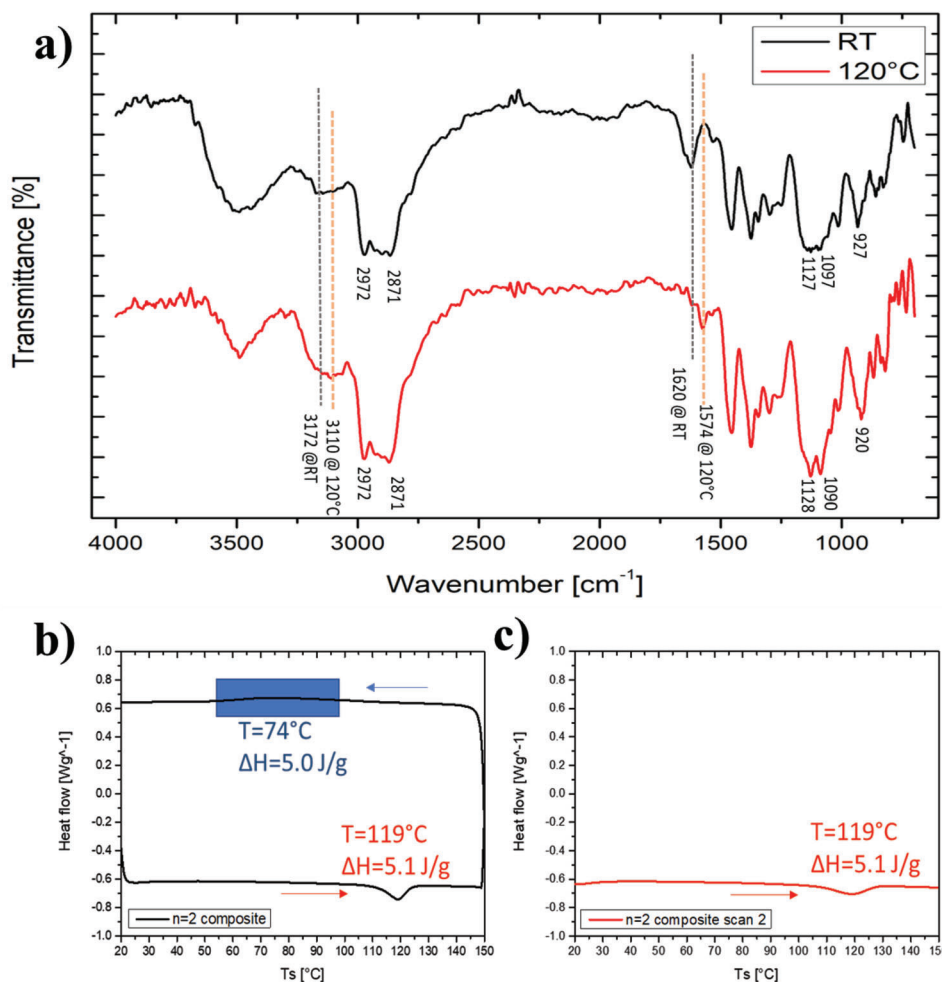


**Figure 3.** a) FT-IR spectra of  $n = 2$  thermochromic composite at room temperature (black line) and  $120\text{ }^{\circ}\text{C}$  (red line). DSC thermograms of the composite  $n = 2$ . b) First heating (bottom), second cooling steps (top), and c) third heating step.

endothermic peak centered at about  $118.5 \pm 0.7\text{ }^{\circ}\text{C}$  during the first heating step, with an onset Temperature ( $T_{\text{onset}}$ ) at around  $111.8 \pm 0.5\text{ }^{\circ}\text{C}$  and a broader exothermic peak centered at about  $74.1 \pm 1.2\text{ }^{\circ}\text{C}$ , with a  $T_{\text{onset}}$  at around  $105.9 \pm 2.0\text{ }^{\circ}\text{C}$ , during the cooling. When the sample is heated again (3<sup>rd</sup> step) the endothermic peak centered at about  $119.0 \pm 2.2\text{ }^{\circ}\text{C}$ , with a  $T_{\text{onset}}$  at around  $106.3 \pm 2.0\text{ }^{\circ}\text{C}$  is again observed. Moreover, the enthalpy value associated with the peak, around  $5\text{ J g}^{-1}$ , is the same in the heating and cooling steps. The observed peaks are consistent with the experimental conditions under which the thermochromic effect is observed for the  $n = 2$  composite (at  $120\text{ }^{\circ}\text{C}$ ) and are attributed to the breaking of the H-bond between MAI/BAI and the Pluronic polymeric chains. Conversely, during cooling the interaction between the perovskite precursors and the polymer chains is restored, resulting in an exothermic reaction that is slower than the endothermic one, confirming the kinetics observed in the thermochromic phenomenon and demonstrating its reversibility. To elucidate the roles of the composite constituents, DSC measurements were conducted on pristine Pluronic (Figure S2, Supporting Information), which showed no peaks in the temperature range explored, highlighting that the thermochromic phe-

nomenon results from the formation and breaking of hydrogen bonds between the MAI/BAI and Pluronic.

Besides the role of hydrogen bonds, another crucial aspect deserves to be considered: an intimate and efficient interaction between polymer and perovskite is desired and this is promoted by the chemistry of the selected materials. In our thermochromic composite, both components exhibit amphiphilic properties: Pluronic L-61 is a nonionic triblock copolymer composed of a central hydrophobic chain of poly(propylene glycol), PPG, flanked by two hydrophilic tails of poly(ethylene glycol), PEG, while 2D PVK has hydrophobic alkyl cations (BA) and hydrophilic inorganic layers ( $\text{PbI}_6^{4-}$ ). It seems that this amphiphilicity is the key element of the working mechanism. Indeed, we observed that by replacing 2D perovskite with a 3D perovskite, which is poor in hydrophobic portions, no significant thermochromic response has been obtained even by increasing the temperature up to  $150\text{ }^{\circ}\text{C}$  (see Figure S3, Supporting Information). This could be due to the chemical incompatibility between Pluronic L-61 and 3D PVK with consequent phase separation that hinders reversible interaction between the two materials. In addition, using PEG, a more hydrophilic polymer than

Pluronic L-61, the formation of a precipitate was observed when the 2D perovskite precursor solution was added to the PEG solution, demonstrating very low affinity between the components. These experiments suggest that the polymer should be a “good solvent” for perovskite.

Finally, we evaluated the rheology of the materials involved and how it changes with temperature. The complex viscosity of the composite based on a perovskite  $n = 2$  at 20 and 120 °C are reported in Figure S4a (Supporting Information), compared with that of pristine Pluronic, Figure S4b (Supporting Information). The higher viscosity observed at room temperature for the composite (2 Pa s), irrespective of the shear strain values, compared to that of Pluronic (0.3 Pa s), can be related to the interactions between the cations and the polymer, according to the FTIR and DSC analysis. At 120 °C, the viscosity of the composite increased over 1000 Pa s due to the formation of the perovskite crystals. The analysis of  $G'$  and  $G''$  moduli (see Figure S5, Supporting Information) showed a change in the rheological behavior of the composite from liquid-like ( $G' < G''$ ) at room temperature to solid-like ( $G' > G''$ ) at 120 °C due to the formation of perovskite crystals, differently from the liquid-like behavior of the pristine Pluronic, irrespective to the temperature and shear strain.

Based on the experiments carried out to investigate the chemistry of our system, we can state that thermochromism in our system is due to the reversible assembly and disassembly of the perovskite performed by the polymer and triggered by temperature. Moreover, we can define the design of an ideal composite, which requires four conditions to be fulfilled simultaneously:

- i. the interaction between the polymeric chains and perovskite building blocks should be energetically favored but not irreversible;
- ii. the polymer must be a “good solvent” for perovskite and therefore must be amphiphilic like 2D perovskite;
- iii. the 2D perovskite domains must be in close contact with the polymer domains, so an adequate polymer/perovskite ratio must be ensured;
- iv. the composite must have “liquid-like” rheological characteristics to facilitate interaction between the polymer chains and the perovskite precursors.

Differently from other previously reported perovskites,<sup>[42,44,45,46,47]</sup> whose performance are shown in Table S3 (Supporting Information) and compared with our system, here the color transition is caused by the reversible interaction between two solid compounds (copolymer and perovskite), as schematically reported in Figure 4, and not between a solid perovskite and a gas (moisture or methylamine). Therefore, the intercalating element is always available inside the thermochromic material, ready to quickly react with the perovskite, without the need to retrieve it from a reservoir or the environment.<sup>[45,46]</sup>

To confirm the perovskite formation in the composite, photoluminescence (PL) measurements and structural characterizations were performed at RT and high temperatures. PL spectra, shown in Figure 5a–c demonstrate that at a low temperature, when the film is transparent, there are no perovskite compounds. On the contrary, at high temperatures, the distinctive peaks of  $(\text{C}_4\text{H}_9\text{NH}_3)_2(\text{CH}_3\text{NH}_3)_{n-1}\text{Pb}_n\text{I}_{3n+1}$  perovskite appear at 521, 616,

and 756 nm for  $n = 1$ ,  $n = 2$ , and  $n = 3$  respectively, showing the well-known redshift in PL caused by the decreasing energy gap of 2D PVK as  $n$  increases.<sup>[33,35,56,59,66]</sup>

Grazing incidence wide-angle scattering measurements (GIWAXS) were performed on composites featuring  $n = 1, 2, 3$  deposited on silicon. The as collected 2D GIWAXS patterns are reported in Figure S6 (Supporting Information), for one sample per each  $n$  value: the resulting 1D-folded profiles are reported in Figure 5d,e. It was verified that at room temperature all films feature mainly an amorphous character, associated with a broad band around  $Q = 0.42 \text{ \AA}^{-1}$  ( $d = 1.5 \text{ nm}$ ), but in  $n = 3$  films crystalline moieties are present as well, producing a few diffraction spots (Figure S6, left-bottom, Supporting Information) leading to the intense diffraction peaks in the 1D-folded profile (Figure 5d) and disappearing upon film heating (Figure 5e). Such peaks are ascribed to crystalline seeds that decompose upon heating, eventually leading to the formation of the layered perovskite, and could be attributed to large crystalline domain size (thus sharp diffraction peaks), bigger than the expected perovskite layer thickness in  $n = 3$ . We infer that in  $n = 3$  composite some intermediate crystalline domains may form at room temperature, by segregation or precipitation at the substrate interface, due to the increasing chemical incompatibility of the perovskite precursors with the Pluronic polymer as  $n$  increases. On the other hand, clear diffraction peaks related to nanoscale periodicity appear upon film heating. In Figure 5e, 1D-folded GIWAXS data are reported, showing the different nanoscale periodicities associated with  $n = 1, 2$ , and 3 perovskite structures. In particular, the out of plane linear cuts are shown: the higher diffracted intensity for the  $n$ -periodicities was indeed detected perpendicular to the film surface, indicating a preferred in-plane orientation of octahedra layers. Based on  $Q$ -positions of diffraction peaks (being  $Q = 4\pi/\lambda \sin\theta$  the scattering vector modulus, and  $\theta$  half the scattering angle), the characteristic periodicities were derived as  $d = 2\pi/Q$ , resulting in  $d_1 = 1.3 \text{ nm}$ ,  $d_2 = 1.9 \text{ nm}$ ,  $d_3 = 2.4 \text{ nm}$ , for films with  $n = 1, 2, 3$ , respectively. As it can be recognized in Figure 5e, peak intensity significantly decreases with increasing  $n$ , so that an enlarged diffraction pattern has been reported in the inset of Figure 5e for the  $n = 3$  sample. Moreover, by reducing the intensity scale, the scattering contribution from the Pluronic polymer becomes evident, as it can be recognized from Figure S7 (Supporting Information), where the diffraction pattern from a bare polymer film is compared to the one from an  $n = 3$  composite film. Figure S7 (Supporting Information) clearly shows how polymer scattering contribution accounts for the baseline of the  $n = 3$  perovskite composite pattern, thus confirming that phase separation phenomena between polymer and perovskite can occur in the case of high- $n$  perovskites. At the same time, it should be noted that the degree of preferred orientation in the heated composites decreases with increasing  $n$  (Figure S6, Supporting Information), leading to clear diffraction spots in the case of  $n = 1$ , and for larger  $n$  to diffraction spots preferentially aligned orthogonally to the film surface, superimposed to continuous diffraction rings ascribed to randomly oriented crystalline domains dispersed in the polymer matrix.

Finally, hysteresis and cyclability tests were carried out on  $(\text{C}_4\text{H}_9\text{NH}_3)_2(\text{CH}_3\text{NH}_3)\text{Pb}_2\text{I}_7$  ( $n = 2$ ) composite to investigate its behavior and stability.

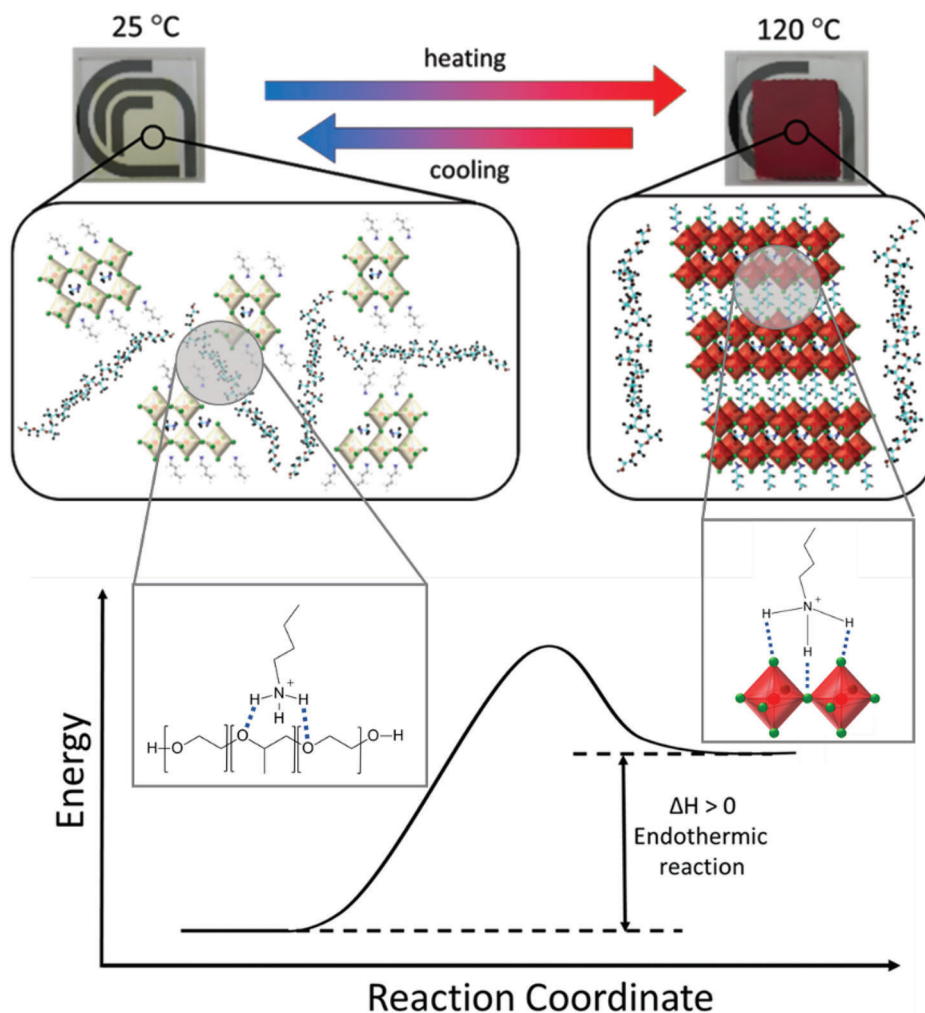


**Figure 4.** Sketch of the suggested working mechanism of polymeric thermochromic composite based on 2D-PVKs (in this case,  $(\text{C}_4\text{H}_9\text{NH}_3)_2(\text{CH}_3\text{NH}_3)\text{Pb}_2\text{I}_7$  ( $n = 2$ )).

The hysteresis diagram (Figure 6a) shows a difference in transition temperature between the heating and cooling processes. The average transition temperature for the heating phase is 86 °C, while the average transition temperature for the cooling phase is 67 °C, with a hysteresis loop of 19 °C, which is consistent with values reported in the literature for other types of perovskite-based thermochromic materials.<sup>[44,45]</sup>

For cyclability test, transmittance at 577 nm was measured every 10 cycles at 25 °C and 120°, respectively. As shown in Figure 6b, after 50 cycles, the sample still maintains a high transmittance variation. Moreover, to provide information on any structural changes occurring in the thermochromic composite upon cycling, we performed GIWAXS and PL measurements on  $n = 2$  samples before and after 50 cycles. The corresponding spectra were added to the Supporting Information (Figure S8a, S8b, and S8c).

By evaluating these data, we can reasonably assume that no degradation phenomena occur and that the composite does not undergo structural changes during the cycles, demon-

strating that the composite can sustain dozens of heating and cooling cycles retaining very good thermochromic capabilities.

### 3. Conclusions

In summary, a new polymeric thermochromic composite based on 2D-PVK was successfully synthesized and deposited by inkjet printing. Through absorption, photoluminescence, and GIWAXS measurements, we were able to figure out that our system changes from an amorphous bleached nonperovskite phase at room temperature to a colored perovskite phase at high temperature. This working mechanism is based on polymer-assisted formation and disassembly of 2D-PVK, as demonstrated by FT-IR, DSC, and rheological measurements.

The composite allows a strong transmittance modulation in a very short time and offers the possibility to tune the color by changing the type of perovskite: it turns from transparent pale-yellow at room temperature to yellow

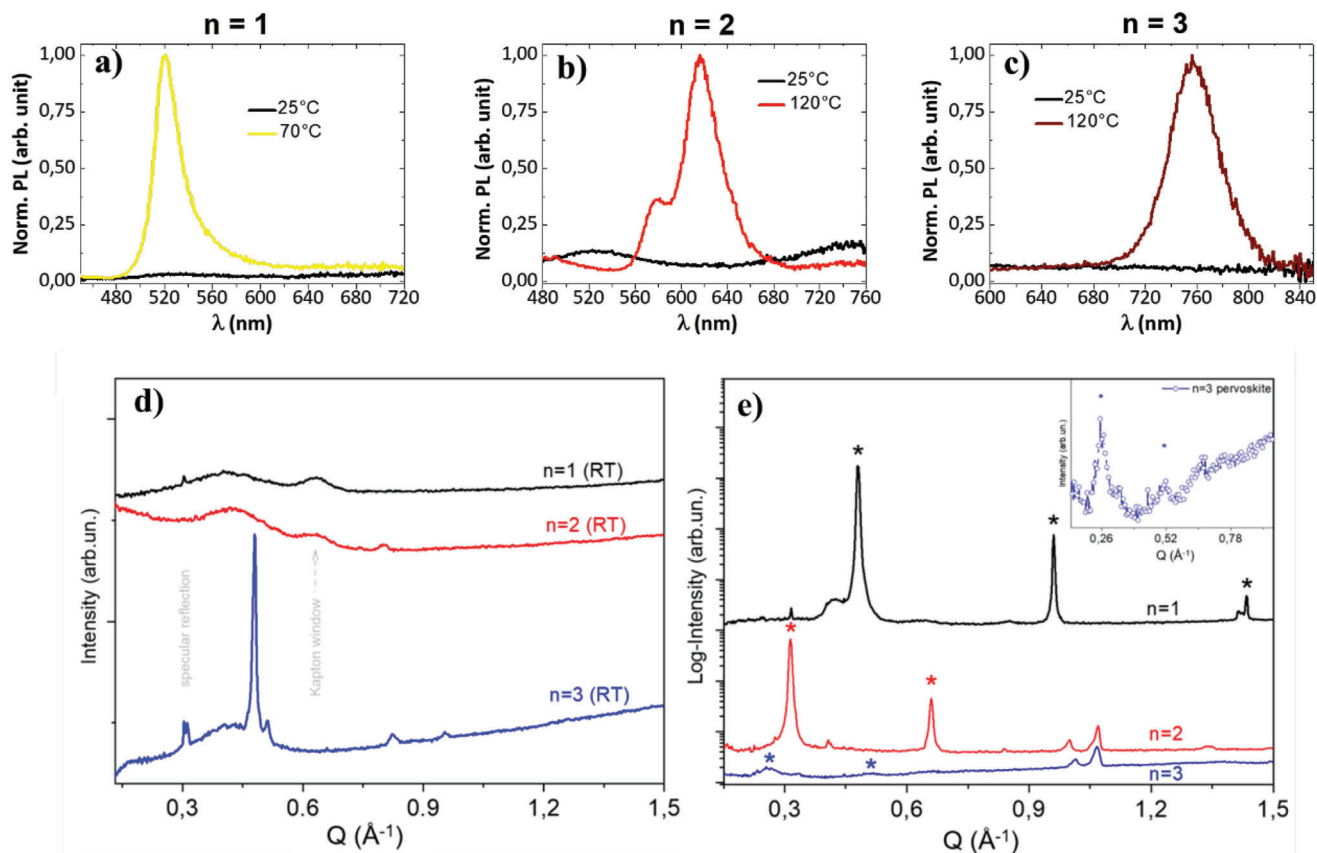


**Figure 5.** Normalized PL spectra of thermochromic  $(C_4H_9NH_3)_2(CH_3NH_3)_{n-1}Pb_nI_{3n+1}$  composite with a)  $n = 1$ , b)  $n = 2$ , and c)  $n = 3$  at two different states, bleached and colored. d) 1D-folded GIWAXS profiles collected at room temperature (RT) for  $n = 1, 2, 3$  perovskite films. e) Out of plane GIWAXS linear cuts collected from  $n = 1, 2, 3$  perovskite films under heating. Inset: close-up of the GIWAXS pattern relevant to the  $n = 3$  film. Equally spaced diffraction peaks related to  $n$ -periodicities are marked by asterisks.

at 70 °C for  $(C_4H_9NH_3)_2PbI_4$  ( $n = 1$ ) and red or brown at 120 °C for  $(C_4H_9NH_3)_2(CH_3NH_3)Pb_2I_7$  ( $n = 2$ ) and  $(C_4H_9NH_3)_2(CH_3NH_3)_2Pb_3I_{10}$  ( $n = 3$ ), respectively.

Moreover, it is easily processed in air, can be deposited on any type of substrate, including flexible ones, and performs

well in any environmental condition, retaining its performance even after dozens of heating and cooling cycles without being encapsulated.

This work provides new insights into the chemistry of thermochromic perovskite materials, overcoming the limits of other

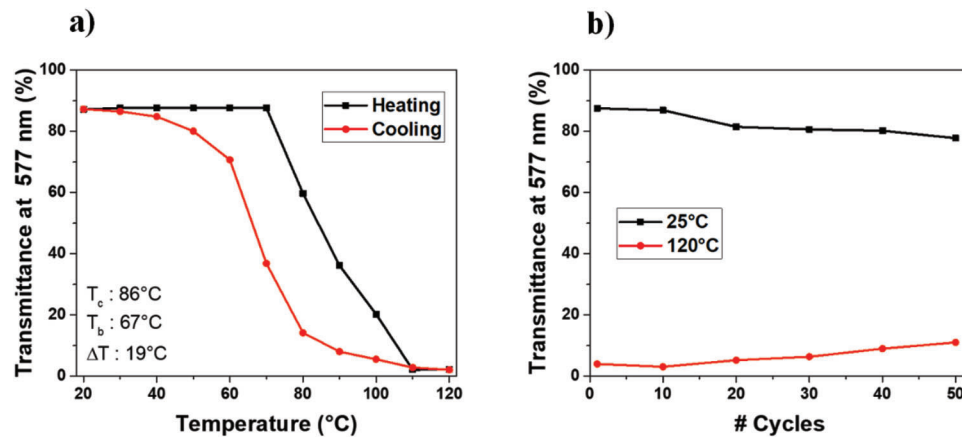


**Figure 6.** a) Hysteresis diagram of  $n = 2$  composite. b) Optical performance (transmittance at 577 nm) at 25 and 120 °C of the  $(C_4H_9NH_3)_2(CH_3NH_3)Pb_2I_7$  ( $n = 2$ ) after 50 cycles.



previously investigated systems, and proposes new efficient and widely applicable alternatives.

## 4. Experimental Section

**Chemicals and Reagents:** Lead(II) iodide ( $\text{PbI}_2$ ), ultradry (99.999% metals basis) was purchased from Alfa Aesar. Methylammonium iodide (MAI,  $\text{CH}_3\text{NH}_3\text{I}$ ) and *n*-Butylammonium iodide (BAI,  $\text{C}_4\text{H}_{12}\text{IN}$ ) were acquired from Greatcell Solar. DMF, THF, DMSO, Poly(ethylene glycol) (PEG, average  $M_n \approx 2000$ ), and Pluronic L-61 (PEG-PPG-PEG, average  $M_n \approx 2000$ ) were purchased from Sigma-Aldrich. All salts and solvents were used as received without any further purification. All chemicals were used as received without any further purification.

**Synthesis:** The polymeric thermochromic composite was prepared by using a solution precursor containing: lead(II) iodide ( $\text{PbI}_2$ ), methylammonium iodide (MAI,  $\text{CH}_3\text{NH}_3\text{I}$ ), *n*-Butylammonium iodide (BAI,  $\text{C}_4\text{H}_{12}\text{IN}$ ), and Pluronic L-61 (PEG-PPG-PEG, average  $M_n \approx 2000$ ) in tetrahydrofuran (THF).

The value of  $n$ , and so 2D-PVK's structure and color of the composite were modified by changing the amounts of perovskite reagents.

**Perovskite Solutions:**  $(\text{BA})_2\text{PbI}_4$  ( $n = 1$ ). 461 mg  $\text{PbI}_2$  and 403 mg *n*-butylammonium iodide were dissolved in a mix of DMF/DMSO (0.8/0.2 mL, respectively) and stirred at 70 °C for 1 h.

$(\text{BA})_2(\text{MA})\text{Pb}_2\text{I}_7$  ( $n = 2$ ). 461 mg  $\text{PbI}_2$ , 80 mg methylammonium iodide, and 201 mg *n*-butylammonium iodide were dissolved in a mix of DMF/DMSO (0.8/0.2 mL, respectively) and stirred at 70 °C for 1 h.

$(\text{BA})_2(\text{MA})_2\text{Pb}_3\text{I}_{11}$  ( $n = 3$ ). 461 mg  $\text{PbI}_2$ , 105 mg methylammonium iodide, and 133 mg *n*-butylammonium iodide were dissolved in a mix of DMF/DMSO (0.8/0.2 mL, respectively) and stirred at 70 °C for 1 h.

$(\text{MA})\text{PbI}_3$  (3D), 461 mg  $\text{PbI}_2$ , and 158.96 mg methylammonium iodide were dissolved in a mix of DMF/DMSO (0.8/0.2 mL, respectively) and stirred at 70 °C for 1 h.

Precursors solutions were prepared in an  $\text{N}_2$ -filled glovebox.

**Thermochromic Inks:** All inks were prepared in air and in a fume hood. For  $(\text{C}_4\text{H}_9\text{NH}_3)_2(\text{CH}_3\text{NH}_3)_{n-1}\text{Pb}_n\text{I}_{3n+1}$  (with  $n = 1, 2$ , and 3) 25  $\mu\text{L}$  of perovskite solution and 63  $\mu\text{L}$  of Pluronic L-61 were dissolved in 0.912 mL of THF, for  $(\text{CH}_3\text{NH}_3)\text{PbI}_3$  (3D) 5  $\mu\text{L}$  of perovskite solution and 63  $\mu\text{L}$  of Pluronic L-61 were dissolved in 0.932 mL of THF. All solution were stirred at room temperature for 1 h.

Thermochromic inks were printed using a new prototype inkjet printer fabricated by T.P.A. s.r.l. and provided with a single-nozzle with a diameter of 300  $\mu\text{m}$ . The printed layers were then transferred on a hot plate and heated at 120 °C for 10 min.

**Inks Characterization:** UV–Vis Transmittance measurements were performed by using a Perkin Elmer UV/Vis/NIR spectrometer (Lambda 1050). A custom-made device with suitable characteristics and dimensions to be integrated into the Perkin Elmer spectrophotometer was built and used to collect transmittance spectra. Its details are reported in the Supporting Information.

Fluorescence spectroscopic studies were performed with an Edinburgh FLS980 spectrometer equipped with a peltier-cooled Hamamatsu R928 photomultiplier tube (185–850 nm), at 25 °C. Corrected spectra were obtained via a calibration curve supplied with the instrument. For the emission spectra, the slits widths were adjusted between 1 and 5 nm, integration time = 0.1 s, 1 nm step. Experimental uncertainties are estimated to be  $\pm 5$  nm for emission peaks.

**Printing Parameters:** The single nozzle printer moves at 1  $\text{m min}^{-1}$  on the fixed glass substrate and ejects drops with a volume of  $\approx 15$  nL from a height of 7 mm above the substrate. Every drop produces a printed dot with a 1.5 mm diameter. The individual circular drops are separated by a distance of 1 mm (center to center). The final printed layers have dimensions of  $16 \times 21$  mm.

**GIWAXS Characterization:** GIWAXS patterns were collected at the XMI-Lab (CNR-IC, Bari), equipped with a rotating anode Fr-E+ Superbright microsource (Cu  $K\alpha$ ) coupled to a SMAX3000 camera (Rigaku).<sup>[67]</sup> The primary X-ray beam size was 200  $\mu\text{m}$ . An Image Plate (IP) detector was

placed at a 87 mm sample-to-detector distance (SDD) and read by off-line RAXIA scanner. Kapton windows were inserted to keep the sample at atmospheric pressure (flight tube at about 0.1 mbar), except for the  $n = 3$  sample measurement at room temperature. Three replicas were analyzed for each  $n$  value. Due to the uneven film surface, the nominal incidence angle resulting in the best signal-to-noise ratio could differ for each sample and was chosen between 1° and 2°. Data collection time was 600 s for each GIWAXS pattern. Patterns were collected before and after sample heating in situ, by using a remote-controlled heater with LabVIEW 2020 software interface, provided by KleisTEK-Advanced Electronic Systems (www.kleisstek.com). Ag Behenate was used as standard material for calibration. Calibration and correction for flat detector projection were performed by the in-house developed software SUNBIM.<sup>[68]</sup>

## Supporting Information

Supporting Information is available from the Wiley Online Library or from the author.

## Acknowledgements

M.C. and C.T.P. contributed equally to this work. This work was supported by the FISR-CNR national project “TECNOMED – Tecnopolo di nanotecnologia e fotonica per la medicina di precisione” – CUP B83B17000010001, by “TecnMed Puglia – Tecnopolo per la medicina di Precisione – Regione Puglia” – CUP B84118000540002, by the MIUR project “ECOTEC – ECO-sustainable and intelligent fibers and fabrics for TECHnic clothing”, PON « R&I» 2014–2020, Project No. ARS01\_00951, CUP B66C18000300005, by the Italian Ministry of Research (MUR) under the complementary actions to the NRRP (PNC0000007) “Fit4MedRob-Fit for Medical Robotics” Grant (Contract No. CUP B53C22006960001), by the European Union – NextGeneration EU project “Network 4 Energy Sustainable Transition—NEST” (Project code PE0000021, CUP B53C22004060006, Concession Decree No. 1561 of 11.10.2022 adopted by Ministero dell'Università e della Ricerca) and by the ERC Consolidator Project No. 101045746—HYNANOSTORE. This work was (partly) supported by the Joint Bilateral Agreement CNR/FAPESP (Brazil) 2022–2023 (No. CUP B57G22000240001). C. Micelli (KleisTEK) is acknowledged for providing the remote-controlled heater and the temperature sensor for in situ experiments. R. Lassandro (CNR-IC) is acknowledged for his technical support in the XMI-lab. Paolo Cazzato (CNR-NANOTEC) is acknowledged for fabricating the customized heater for in situ absorption and photoluminescence measurements.

## Conflict of Interest

The authors declare no conflict of interest.

## Data Availability Statement

The data that support the findings of this study are available from the corresponding author upon reasonable request.

## Keywords

2D perovskites, hybrid organic–inorganic perovskites, optical devices, thermochromic materials, thermoresponsive thin films

Received: July 28, 2023

Revised: September 12, 2023

Published online: November 27, 2023

- [1] R. Kulcar, M. Friskovec, M. K. Gunde, N. Knesarek, *Color. Technol.* **2011**, *127*, 411.
- [2] R. Kulcar, M. Friskovec, N. Hauptman, A. Vesel, M. K. Gunde, *Dyes Pigments* **2010**, *86*, 271.
- [3] Y. Guan, L. Zhang, D. Wang, J. L. West, S. Fu, *Mater. Des.* **2018**, *147*, 28.
- [4] K. R. Karpagam, K. S. Saranya, J. Gopinathan, A. Bhattacharyya, *J. Text. Inst.* **2017**, *108*, 1122.
- [5] L. S. Ribeiro, T. Pinto, A. Monteiro, O. S. G. P. Soares, C. Pereira, C. Freire, M. F. R. Pereira, *J. Mater. Sci.* **2013**, *48*, 5085.
- [6] C. G. Schäfer, C. Lederle, K. Zentel, B. Stühn, M. Gallei, *Macromol. Rapid Commun.* **2014**, *35*, 1852.
- [7] L. Hairong, J. Ming, L. Qi, *Polym. Compos.* **2014**, *35*, 2154.
- [8] S. Zheng, Y. Xu, Q. Shen, H. Yang, *Sol. Energy* **2015**, *112*, 263.
- [9] M. Basson, T. S. Pottebaum, *Exp. Fluids* **2012**, *53*, 803.
- [10] O. Mapazi, P. K. Matabola, R. M. Moutloali, C. J. Ngila, *Sens. Actuators B, Chem.* **2017**, *252*, 671.
- [11] J. Sun, H. Wang, L. Wang, H. Cao, H. Xie, X. Luo, *Smart Mater. Struct.* **2014**, *23*, 125038.
- [12] A. J. J. Kragt, N. C. M. Zuurbier, D. J. Broer, A. P. H. J. Schenning, *ACS Appl. Mater. Interfaces* **2019**, *11*, 28172.
- [13] A. Seeboth, *Chin. J. Polym. Sci.* **2006**, *24*, 363.
- [14] W. Zhang, X. Ji, C. Zeng, K. Chen, Y. Yin, C. Wang, *J. Mater. Chem. C* **2017**, *5*, 8169.
- [15] S. Wang, M. Liu, L. Kong, Y. Long, X. Jiang, A. Yu, *Prog. Mater. Sci.* **2016**, *81*, 1.
- [16] Y. Gao, S. Wang, L. Kang, Z. Chen, J. Du, X. Liu, H. Luo, M. Kanehira, *Energy Environ. Sci.* **2012**, *5*, 8234.
- [17] M. Li, S. Magdassi, Y. Gao, Y. Long, *Small* **2017**, *13*, 1701147.
- [18] M. K. Dietrich, F. Kuhl, A. Polity, P. J. Klar, *Appl. Phys. Lett.* **2017**, *110*, 141907.
- [19] S. Y. Li, G. A. Niklasson, C. G. Granqvist, *J. Appl. Phys.* **2014**, *115*, 053513.
- [20] L. Kang, Y. Gao, H. Luo, Z. Chen, J. Du, Z. Zhang, *ACS Appl. Mater. Interfaces* **2011**, *3*, 135.
- [21] C. Liu, I. Balin, S. Magdassi, I. Abdulhalim, Y. Long, *Opt. Express* **2015**, *23*, A124.
- [22] Q. Lu, C. Liu, N. Wang, S. Magdassi, D. Mandler, Y. Long, *J. Mater. Chem. C* **2016**, *4*, 8385.
- [23] S. Liu, H. Fang, Y. Su, J. Hsieh, *Jpn. J. Appl. Phys.* **2014**, *53*, 063201.
- [24] M. Jiang, X. Cao, S. Bao, H. Zhou, P. Jin, *Thin Solid Films* **2014**, *562*, 314.
- [25] D. Vernardou, D. Louloudakis, E. Spanakis, N. Katsarakis, E. Koudoumas, *Sol. Energy Mater. Sol. Cells* **2014**, *128*, 36.
- [26] M. E. A. Warwick, I. Ridley, R. Binions, *J. Nanosci. Nanotechnol.* **2011**, *11*, 8158.
- [27] D. C. Maclaren, M. A. White, *J. Mater. Sci.* **2005**, *40*, 669.
- [28] C. F. Zhu, A. B. Wu, *Thermochim. Acta* **2005**, *425*, 7.
- [29] H. Oda, *Dyes Pigments* **2005**, *66*, 103.
- [30] Z. Yang, H. Peng, W. Wang, T. Liu, *J. Appl. Polym. Sci.* **2009**, *116*, 2658.
- [31] Y. Liu, S. Akin, L. Pan, R. Uchida, N. Arora, J. V. Milić, A. Hinderhofer, F. Schreiber, A. R. Uhl, S. M. Zakeeruddin, A. Hagfeldt, M. Ibrahim Dar, M. Grätzel, *Sci. Adv.* **2019**, *5*, eaaw2543.
- [32] W. S. Yang, B.-W. Park, E. H. Jung, N. J. Jeon, Y. C. Kim, D. U. Lee, S. S. Shin, J. Seo, E. K. Kim, J. H. Noh, S. Il Seok, *Science* **2017**, *356*, 1376.
- [33] D. H. Cao, C. C. Stoumpos, O. K. Farha, J. T. Hupp, M. G. Kanatzidis, *J. Am. Chem. Soc.* **2015**, *137*, 7843.
- [34] Y. Lee, J. Kwon, E. Hwang, C.-H. Ra, W. J. Yoo, J.-H. Ahn, J. H. Park, J. H. Cho, *Adv. Mater.* **2015**, *27*, 41.
- [35] K. Wang, C. Wu, D. Yang, Y. Jiang, S. Priya, *ACS Nano* **2018**, *12*, 4919.
- [36] Z.-K. Tan, R. S. Moghaddam, M. L. Lai, P. Docampo, R. Higler, F. Deschler, M. Price, A. Sadhanala, L. M. Pazos, D. Credgington, F. Hanusch, T. Bein, H. J. Snaith, R. H. Friend, *Nat. Nanotechnol.* **2014**, *9*, 687.
- [37] A. Fieramosca, L. Polimeno, V. Ardzzone, L. De Marco, M. Pugliese, V. Maiorano, M. De Giorgi, L. Dominici, G. Gigli, D. Gerace, D. Ballarini, D. Sanvitto, *Sci. Adv.* **2019**, *5*, eaav9967.
- [38] R. Su, C. Diederichs, J. Wang, T. C. H. Liew, J. Zhao, S. Liu, W. Xu, Z. Chen, Q. Xiong, *Nano Lett.* **2017**, *17*, 3982.
- [39] A. Fieramosca, L. De Marco, M. Passoni, L. Polimeno, A. Rizzo, B. L. T. Rosa, G. Cruciani, L. Dominici, M. De Giorgi, G. Gigli, L. C. Andreani, D. Gerace, D. Ballarini, D. Sanvitto, *ACS Photonics* **2018**, *5*, 4179.
- [40] L. Polimeno, A. Fieramosca, G. Lerario, M. Cinquino, M. De Giorgi, D. Ballarini, F. Todisco, L. Dominici, V. Ardzzone, M. Pugliese, C. T. Prontera, V. Maiorano, G. Gigli, L. De Marco, D. Sanvitto, *Adv. Opt. Mater.* **2020**, *8*, 2000176.
- [41] M. Cinquino, L. Polimeno, G. Lerario, M. De Giorgi, A. Moliterni, V. Olieric, A. Fieramosca, S. Carallo, R. Mastria, V. Ardzzone, L. Dominici, D. Ballarini, C. Giannini, D. Sanvitto, A. Rizzo, L. De Marco, *J. Lumin.* **2020**, *221*, 117079.
- [42] J. Lin, M. Lai, L. Dou, C. S. Kley, H. Chen, F. Peng, J. Sun, D. Lu, S. A. Hawks, C. Xie, F. Cui, A. P. Alivisatos, D. T. Limmer, P. Yang, *Nat. Mater.* **2018**, *17*, 261.
- [43] M. De Bastiani, M. I. Saidaminov, I. Dursun, L. Sinatra, W. Peng, U. Buttner, O. F. Mohammed, O. M. Bakr, *Chem. Mater.* **2017**, *29*, 3367.
- [44] Y. Zhang, C. Y. Tso, J. S. Iñigo, S. Liu, H. Miyazaki, C. Y. H. Chao, K. M. Yu, *Appl. Energy* **2019**, *254*, 113690.
- [45] S. Liu, Y. W. Du, C. Y. Tso, H. H. Lee, R. Cheng, S. P. Feng, K. M. Yu, *Adv. Funct. Mater.* **2021**, *31*, 2010426.
- [46] L. M. Wheeler, D. T. Moore, R. Ihly, N. J. Stanton, E. M. Miller, R. C. Tenent, J. L. Blackburn, N. R. Neale, *Nat. Commun.* **2017**, *8*, 1722.
- [47] Y. Zhang, Z. Wang, S. Hu, P. Yan, H. Li, C. X. Sheng, *ACS Appl. Mater. Interfaces* **2021**, *4*, 12042.
- [48] C. Pareja-Rivera, D. Solis-Ibarra, *Adv. Opt. Mater.* **2021**, *9*, 2100633.
- [49] A. Singh, S. Satapathi, *Adv. Opt. Mater.* **2021**, *9*, 2101062.
- [50] W. Ning, X. G. Zhao, J. Klarbring, S. Bai, F. Ji, F. Wang, S. I. Simak, Y. Tao, X. M. Ren, L. Zhang, W. Huang, I. A. Abrikosov, F. Gao, *Adv. Funct. Mater.* **2019**, *29*, 1807375.
- [51] A. Halder, D. Choudhury, S. Ghosh, A. S. Subbiah, S. K. Sarkar, *J. Phys. Chem. Lett.* **2015**, *6*, 3180.
- [52] B. A. Rosales, J. Kim, V. M. Wheeler, L. E. Crowe, K. J. Prince, M. Mirzokarimov, T. Daligault, A. Duell, C. A. Wolden, L. T. Schelhas, L. M. Wheeler, *Adv. Energy Mater.* **2023**, *13*, 2203331.
- [53] I. C. Smith, E. T. Hoke, D. Solis-Ibarra, M. D. McGehee, H. I. Karunadasa, *Angew. Chem., Int. Ed.* **2014**, *53*, 11232.
- [54] A. Coriolano, L. Polimeno, M. De Giorgi, F. Todisco, R. Mastria, V. Ardzzone, L. Dominici, D. Ballarini, A. Rizzo, G. Gigli, D. Sanvitto, L. De Marco, *Nanomaterials* **2021**, *11*, 465.
- [55] M. D. Smith, B. A. Connor, H. I. Karunadasa, *Chem. Rev.* **2019**, *119*, 3104.
- [56] M. Cinquino, A. Fieramosca, R. Mastria, L. Polimeno, A. Moliterni, V. Olieric, N. Matsugaki, R. Panico, M. De Giorgi, G. Gigli, C. Giannini, A. Rizzo, D. Sanvitto, L. De Marco, *Adv. Mater.* **2021**, *33*, 2102326.
- [57] C. M. Raghavan, T.-P. Chen, S.-S. Li, W.-L. Chen, C.-Y. Lo, Y.-M. Liao, G. Haider, C.-C. Lin, C.-C. Chen, R. Sankar, Y.-M. Chang, F.-C. Chou, C.-W. Chen, *Nano Lett.* **2018**, *18*, 3221.
- [58] C. C. Stoumpos, D. H. Cao, D. J. Clark, J. Young, J. M. Rondinelli, J. I. Jang, J. T. Hupp, M. G. Kanatzidis, *Chem. Mater.* **2016**, *28*, 2852.
- [59] G. Grancini, M. K. Nazeeruddin, *Nat. Rev. Mater.* **2019**, *4*, 4.
- [60] M. Fahad, M. Gilbert, P. Dickens, *Plast. Rubber Compos.* **2012**, *41*, 148.
- [61] T. Al Kayal, D. Panetta, B. Canciani, P. Losi, M. Tripodi, S. Burchielli, P. Ottoni, P. A. Salvadori, G. Soldani, *PLoS One* **2015**, *10*, 0125110.
- [62] S. Yuan, Z.-K. Wang, L.-X. Xiao, C.-F. Zhang, S.-Y. Yang, B.-B. Chen, H.-T. Ge, Q.-S. Tian, Y. Jin, L.-S. Liao, *Adv. Mater.* **2019**, *31*, 1904319.
- [63] J. Joseph, E. D. Jemmis, *J. Am. Chem. Soc.* **2007**, *129*, 4620.

- [64] Z. Ren, J. Yu, Z. Qin, J. Wang, J. Sun, C. C. S. Chan, S. Ding, K. Wang, R. Chen, K. S. Wong, X. Lu, W.-J. Yin, W. C. H. Choy, *Adv. Mater.* **2021**, *33*, 2005570.
- [65] B. A. Rosales, L. E. Mundt, T. G. Allen, D. T. Moore, K. J. Prince, C. A. Wolden, G. Rumbles, L. T. Schelhas, L. M. Wheeler, *Nat. Commun.* **2020**, *11*, 5234.
- [66] W. Paritmongkol, N. S. Dahod, A. Stollmann, N. Mao, C. Settens, S.-L. Zheng, W. A. Tisdale, *Chem. Mater.* **2019**, *31*, 5592.
- [67] D. Altamura, R. Lassandro, F. A. Vittoria, L. De Caro, D. Siliqi, M. Ladisa, C. Giannini, *J. Appl. Crystallogr.* **2012**, *45*, 869.
- [68] D. Siliqi, L. De Caro, M. Ladisa, F. Scattarella, A. Mazzone, D. Altamura, T. Sibillano, C. Giannini, *J. Appl. Crystallogr.* **2016**, *49*, 1107.